

An Additive Manufacturing Part Qualification Framework: Transferring Knowledge of Stress-strain Behaviors from Additively Manufactured Polymers to Metals

Chenglong Duan¹ and Dazhong Wu^{1,*}

¹Department of Mechanical and Aerospace Engineering, College of Engineering and Computer Science, University of Central Florida, Orlando, FL 32816, USA

* Corresponding author
Email: dazhong.wu@ucf.edu

Abstract

Part qualification is crucial in additive manufacturing (AM) because it ensures that additively manufactured parts can be consistently produced and reliably used in critical applications. Part qualification aims at verifying that an additively manufactured part meets performance requirements; therefore, predicting the complex stress-strain behaviors of additively manufactured parts is critical. We develop a dynamic time warping (DTW)-transfer learning (TL) framework for additive manufacturing part qualification by transferring knowledge of the stress-strain behaviors of additively manufactured low-cost polymers to metals. Specifically, the framework employs DTW to select a polymer dataset as the source domain that is the most relevant to the target metal dataset. Using a long short-term memory (LSTM) model, four source polymers (i.e., Nylon, PLA, CF-ABS, and Resin) and three target metals (i.e., AlSi10Mg, Ti6Al4V, and carbon steel) that are fabricated by different AM techniques are utilized to demonstrate the effectiveness of the DTW-TL framework. Experimental results show that the DTW-TL framework identifies the closest match between polymers and metals to select one single polymer dataset as the source domain. The DTW-TL model achieves the lowest mean absolute percentage error of 12.41% and highest coefficient of determination of 0.96 when three metals are used as the target domain, respectively, outperforming the vanilla LSTM model without TL as well as the TL model pre-trained on four polymer datasets as the source domain.

Keywords: Part qualification; Additive manufacturing; Stress-strain behaviors; Transfer learning; Dynamic time warping.

1. Introduction

Additive manufacturing (AM) has a wide range of applications in aerospace, automotive, energy, defense, and medical industries [1-5]. Metal AM, in particular, have become a focus area due to their superior mechanical properties for high-performance applications [6-8]. However, metal AM has not been widely adopted in critical applications due to defects induced by processes and uncertainty in the mechanical behavior of additively manufactured parts [9-11]. Therefore, part qualification is crucial in metal AM because it verifies that additively manufactured parts satisfy the required design specifications to ensure these parts can be consistently reproduced, scaled for mass production, and reliably used in critical applications [12, 13]. Predicting the complex stress-strain behaviors of additively manufactured metal parts is one of the critical steps in part qualification since the stress-strain behavior describes the mechanical behavior of materials under varying design and AM process parameters [14].

Conventional part qualification techniques, which involve destructive and non-destructive testing (NDT), are limited in their ability to predict the complex stress-strain behaviors of additively manufactured parts. Destructive testing such as tensile or compression tests are labor-intensive and expensive. NDT techniques include in-process monitoring and post-process qualification. However, in-process monitoring often requires expensive measurement techniques such as thermal imaging or in-situ X-ray. Therefore, with the recent advances in artificial intelligence (AI) and machine learning (ML), data-driven methods have been

increasingly used to predict the stress-strain behavior of additively manufactured materials with high accuracy and efficiency [15-18]. For example, Liu et al. [18] proposed two feature representation approaches for convolutional neural networks (CNN) to predict the stress-strain behaviors of additively manufactured lattices structures.

Training an effective ML model often requires large volumes of labeled data, which is costly and time consuming, particularly for additively manufactured metals [19, 20]. Specifically, the raw metal powders required for laser-based metal AM can cost between \$50 and \$600 per kilogram. And the cost of metal AM machinery typically exceeds \$10,000. But for polymer AM machinery, its cost can be lower than \$500. Meanwhile, common polymer filaments cost only \$20 to \$50 per kilogram. Therefore, most of the studies only focus on how to predict the stress-strain behaviors of additively manufactured polymers. Further, conventional ML models are not generalizable when material, geometry, and process condition vary. To address this issue, transfer learning (TL) emerges as a potential solution by transferring knowledge from more abundant and cheaper datasets, such as the dataset collected from polymers, thereby significantly reducing the amount of required metal data [21, 22].

However, directly increasing the dataset size in the source domain does not necessarily improve predictive performance [23, 24]. In fact, adding more training data in the source domain that are less relevant to the target domain may result in poor predictive performance [25, 26]. Therefore, selecting the source domain that is most relevant to the target domain from a pool of potential source domains is crucial to the performance of a TL model. In this context, dynamic time warping (DTW), a widely used method for measuring similarity between time-series data [27, 28], can be used to quantify the difference between stress-strain curves of polymers and metals. By capturing similarities and differences in curve shapes, even when stress-strain curves are misaligned in the strain or stress scale because of the differences between polymers and metals, DTW can provide a powerful method for objectively selecting the most relevant polymer dataset to serve as the source domain.

To address the aforementioned issues, a novel DTW-TL framework was developed to predict the stress-strain behaviors of additively manufactured metals under tensile loads by transferring knowledge from low-cost additively manufactured polymers. By firstly using DTW to identify which source polymer exhibited the highest similarity (i.e., the minimum DTW distance) to a target metal, the source domain only contained data from the selected polymer. Subsequently, a long short-term memory (LSTM) model was pre-trained on the selected polymer dataset, and then the model was fine-tuned on the target domain training dataset. Specifically, the source domain contained data from four polymers, including Nylon (Ultimaker), polylactic acid (PLA, MatterHackers), carbon fiber-acrylonitrile butadiene styrene (CF-ABS, Push Plastic), and photopolymer resin (Resin, Flashforge). Nylon, PLA, and CF-ABS samples were fabricated by fused filament fabrication (FFF) and Resin samples were fabricated by digital light processing (DLP). The target domain contained data from three metals, including AlSi10Mg (3D Systems, Inc), Ti6Al4V (3D Systems, Inc), and carbon steel (Böhler welding). AlSi10Mg and Ti6Al4V samples were fabricated by laser powder bed fusion (L-PBF), and carbon steel samples were fabricated by wire and arc additive manufacturing (WAAM). Experimental results showed that DTW-TL model using only one selected polymer dataset as the source domain achieves higher predictive performance compared to vanilla LSTM model without TL and TL model using all four polymer datasets as the source domain. The main contributions of this study are summarized as follows:

- (1) A generic dynamic time warping-transfer learning framework was developed to predict the stress-strain behaviors of additively manufactured metals by transferring knowledge from low-cost additively manufactured polymers.
- (2) A dynamic time warping-based source domain selection process was developed to quantitatively evaluate the similarity between the stress-strain behaviors of source and target domain datasets as well as select the optimal source domain dataset which is the most relevant to target domain.

(3) A comprehensive dataset including four additively manufactured polymers and three additively manufactured metals was used to demonstrate the effectiveness of the dynamic time warping-transfer learning framework.

2. Material and methods

2.1 Transfer learning framework

Fig. 1 illustrates the DTW-TL framework for predicting the stress-strain behaviors of additively manufactured metals by transferring knowledge from low-cost additively manufactured polymers. First, in Fig. 1a, the stress-strain curves (ϵ represents for strain and σ represents for stress) of several polymers (i.e., Nylon, PLA, CF-ABS, and Resin) from the source domain are compared with the curves of metals (i.e., AlSi10Mg, Ti6Al4V, and carbon steel) from the target domain training dataset via DTW to identify the source polymer whose stress-strain behavior is the most similar in shape to the target metal (i.e., minimum DTW distance). This selected polymer dataset is then used to pre-train a LSTM model. Specifically, in Fig. 1b, the polymer dataset is split into an input matrix and a corresponding output vector. Each input matrix consists of a sequence of strain values (ϵ^t , time-variant) along with constant process parameters (P , time-invariant) concatenated at each time step. Each output vector consists of the stress values at each time step (σ^t , time-variant).

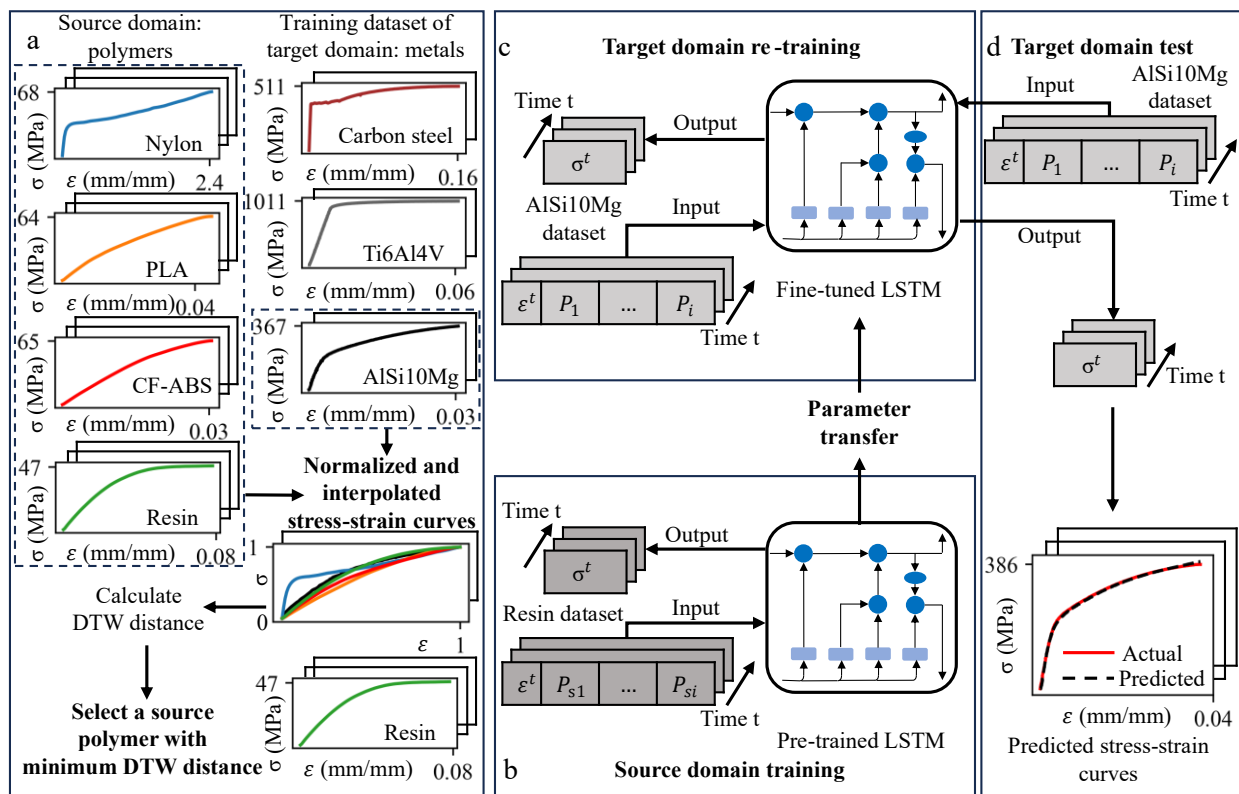


Fig. 1. Overview of the DTW-TL framework. (a) DTW-based source domain selection process. (b) Pre-train a LSTM model on the source domain dataset which only consists of a polymer dataset with minimum DTW distance. (c) Fine-tune the pre-trained LSTM model on the target domain training dataset. (d) Predict stress-strain behaviors on the target domain test dataset.

Second, the parameters of pre-trained model are transferred to another LSTM model, which is then fine-tuned using stress-strain data and corresponding process parameters of the target domain training dataset. In this study, the parameter transfer strategy is used because it allows the target model to start from a favorable position, where the model have already captured useful features and knowledge from the source

domain. Fine-tuning then adjusts the model parameters to better fit the target data, often resulting in faster convergence and improved performance, particularly when the size of the target dataset is limited. In the parameter transfer process, model parameters of the pre-trained LSTM can be denoted as θ_s . For the target model, we initialize its parameters θ_t with those from the source model

$$\theta_t^0 = \theta_s \quad (1)$$

The target model is then fine-tuned using the training data of the target domain by minimizing a loss function L_t , this fine-tuning process is iteratively performed as follows

$$\theta_t^{k+1} = \theta_t^k - \eta \nabla_{\theta} L_t(\theta_t^k) \quad (2)$$

where θ_t^k represents the target model parameters at iteration k , η is the learning rate, and $\nabla_{\theta} L_t(\theta_t^k)$ is the gradient of the loss function with respect to the parameters. Finally, in Fig. 1d, the fine-tuned LSTM model is validated on the target domain test dataset. Fig. 1 only shows the DTW-TL process to predict the stress-strain behaviors of the AlSi10Mg samples, the process for predicting the stress-strain behaviors of the Ti6Al4V and carbon steel samples are the same.

For the LSTM model used in this work, it was originally evolved from the recurrent neural network (RNN) [29]. By incorporating a gate-controlled memory cell, LSTM is designed to handle the long-term dependency problem often encountered in sequential tasks. Fig. 2a shows a layered LSTM architecture with an input layer, an LSTM layer consisting of multiple LSTM cells, a flatten layer, a fully connected layer, and an output layer. At each time step x^t , the input flows into an LSTM cell, enabling the network to learn temporal dependencies. The outputs of the LSTM layer then pass into a flatten layer, which converts the data into a one-dimensional vector suitable for processing in the fully connected layer. Ultimately, this fully connected layer yields predictions at each time step, forming the output layer.

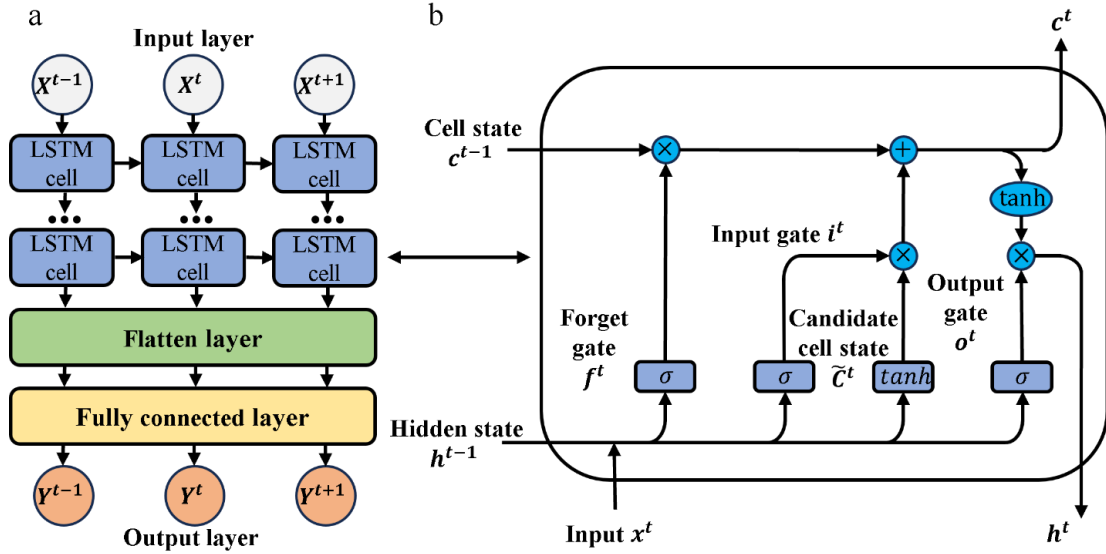


Fig. 2. Architecture of a typical LSTM model. (a) A layered LSTM model. (b) Structure of the LSTM cell.

Fig. 2b depicts the internal architecture of a single LSTM cell, highlighting how it mitigates the vanishing or exploding gradient problems typical of standard RNNs. The core component is the cell state c^t , which acts as a memory capable of storing information over extended time steps. Three gates include forget gate f^t , input gate i^t , and output gate o^t , controlling the flow of information into and out of the cell state. The forget gate determines how much of the previous cell state c^{t-1} should be retained, while the input gate decides the degree to which new candidate information \tilde{c}^t updates the current cell state. Finally, the output

gate governs how much of the updated cell state is revealed as the hidden state h^t at the current time step. Moreover, in the LSTM cell diagram, symbols \otimes and \oplus indicate pointwise multiplication and addition, respectively, while the σ_{sig} represent the sigmoid activation and the \tanh block represents the hyperbolic tangent function. Mathematically, the forward-propagation procedure for an LSTM with a forget gate can be expressed as in Eqs. (3)-(8), where W_{fh} , W_{fx} , W_{ih} , W_{ix} , W_{ch} , W_{cx} , W_{oh} , and, W_{ox} are the weight matrices for each of the gates, and b_f , b_i , b_c , b_o are their respective biases. These learnable parameters allow the network to adapt its memory mechanism to the specific temporal patterns in training data, effectively capturing long-term dependencies during backpropagation.

$$\text{Forget gate } f^t = \sigma_{sig}(W_{fh}h^{t-1} + W_{fx}x^t + b_f) \quad (3)$$

$$\text{Input gate } i^t = \sigma_{sig}(W_{ih}h^{t-1} + W_{ix}x^t + b_i) \quad (4)$$

$$\text{Candidate cell state } c^t = f^t * c^{t-1} + i^t * \tilde{C}^t \quad (5)$$

$$\text{Memory cell state } \tilde{C}^t = \tanh(W_{ch}h^{t-1} * W_{cx}x^t + b_c) \quad (6)$$

$$\text{Output gate } o^t = \sigma_{sig}(W_{oh}o^{t-1} + W_{ox}x^t + b_o) \quad (7)$$

$$\text{Hidden state } h^t = o^t * \tanh(c^t) \quad (8)$$

In this study, the LSTM model was built using PyTorch and was trained on a computer equipped with an NVIDIA GeForce RTX 4090 GPU, an Intel i9 14900KF CPU, and 32 GB of RAM. The model consists of one LSTM layer that contains 32 hidden units, followed by a fully connected layer that maps the final hidden state to a single stress output. Moreover, since stress-strain curves are time-series data, the sequence length is crucial when design the LSTM input structure. For a sequence length n , the input from the n sequential data points (strain and parameters) are combined to predict the $(n + 1)$ -th stress.

Several error metrics, including mean absolute percentage error (MAPE), root mean squared error (RMSE), and coefficient of determination (R^2), are used to evaluate the performance of the model. The MAPE indicates the relative error, expressed as a percentage. The RMSE is a quadratic scoring rule that measures the square root of the average of squared differences, especially sensitive for large differences. R^2 also known as the coefficient of determination, measures the proportion of the variance in the dependent variable that is predictable from the independent variable. These error metrics are defined as follows

$$MAPE (\%) = \frac{\sum_{i=1}^n \frac{|y_i - \hat{y}_i|}{y_i}}{n} \times 100 \quad (9)$$

$$RMSE = \sqrt{\frac{\sum_{i=1}^n (y_i - \hat{y}_i)^2}{n}} \quad (10)$$

$$R^2 = 1 - \frac{\sum_{i=1}^n (y_i - \hat{y}_i)^2}{\sum_{i=1}^n (y_i - \bar{y})^2} \quad (11)$$

where n is the number of data points, y_i is the actual value, \hat{y}_i is the predicted value, \bar{y} is the mean of actual value.

2.2 Dynamic time warping-based source domain selection process

Although polymers and metals exhibit varying microstructures and mechanical properties, certain stress-strain features, such as initial elastic response, can share partially similar patterns to facilitate the TL process. However, it is challenging to quantify the similarity of the raw stress-strain curves of polymers and metals because of the substantial differences in their stress and strain scales. Therefore, prior to applying any distance metric, it is critical to normalize and align the stress-strain curves for fair comparison. After normalization, several distance metrics can be considered: (i) Euclidean distance treats each curve as a long vector and sums point-by-point squared errors, which means it ignores the curve as a whole and over-penalizes even slight shifts. (ii) Pearson correlation coefficient captures whether the curves rise and fall together but misses the shifts along the strain axis. (iii) Fréchet distance, which measures the minimal

leash length needed to traverse both curves, allows some misalignment but is slow to compute and sensitive to outliers. By contrast, DTW deliberately stretches or compresses one curve along the strain axis to align important mechanical behaviors. This makes DTW much better at matching overall shape and local features.

Therefore, DTW is integrated into our framework, offering a robust method to handle non-linear temporal or strain-axis misalignments, thereby enabling more accurate cross-material similarity assessments. Specifically, DTW process treats the entire stress-strain curve as a single functional entity to compare overall curve shapes rather than independent vectors of stress and strain. The output after the process is a scalar distance, often referred to as the DTW distance. This distance captures how much one curve must be warped (stretched or compressed along the strain axis) to match another. A smaller DTW distance indicates that the two stress-strain curves are more similar, a larger distance implies more differences.

Here we briefly introduce the DTW-based source domain selection process in this study by mathematical formulations [28, 30]. Suppose that we have two stress-strain curves, one is the polymer curve $P = \{(\epsilon_p^i, \sigma_p^i)\}_{i=1}^{N_p}$, where ϵ_p^i is the strain and σ_p^i is the stress for the i -th point, and N_p is the number of points, the other one is the metal curve $M = \{(\epsilon_m^i, \sigma_m^i)\}_{i=1}^{N_m}$, where ϵ_m^i is the strain and σ_m^i is the stress for the i -th point, and N_m is the number of points. First, to make these two curves comparable over the same axis, normalize the strain and stress values for both two curves to a range of [0,1] by dividing their corresponding max values, resulting in normalized curves $\tilde{P} = \{(\tilde{\epsilon}_p^i, \tilde{\sigma}_p^i)\}_{i=1}^{N_p}$ and $\tilde{M} = \{(\tilde{\epsilon}_m^i, \tilde{\sigma}_m^i)\}_{i=1}^{N_m}$.

$$\tilde{\epsilon}_p^i = \frac{\epsilon_p^i}{\max(\epsilon_p)}, \tilde{\sigma}_p^i = \frac{\sigma_p^i}{\max(\sigma_p)}, \tilde{\epsilon}_m^i = \frac{\epsilon_m^i}{\max(\epsilon_m)}, \tilde{\sigma}_m^i = \frac{\sigma_m^i}{\max(\sigma_m)} \quad (12)$$

Second, a strain grid $\{\epsilon_c^i\}_{i=1}^N$ is defined to interpolate stress values for both curves, where ϵ_c^i is evenly spaced in [0,1] with N points. Specifically, the value of N is 120, therefore, the interpolated polymer curve is $P_c = \{(\tilde{\epsilon}_p^k, \tilde{\sigma}_p^k)\}_{k=1}^{120}$ and the interpolated metal curve is $M_c = \{(\tilde{\epsilon}_m^l, \tilde{\sigma}_m^l)\}_{l=1}^{120}$. Then, the local distance is obtained, where each element represents the squared difference between the k -th and l -th stress values from the interpolated polymer and metal curves, respectively

$$d(k, l) = (\tilde{\sigma}_p^k - \tilde{\sigma}_m^l)^2 \quad (13)$$

Third, the cumulative cost matrix D is constructed to represent the minimal cumulative cost of aligning the k -th point of the polymer curve to the l -th point of the metal curve. The recurrence relation is

$$D(k, l) = d(k, l) + \min [D(k-1, l), D(k, l-1), D(k-1, l-1)] \quad (14)$$

subject to boundary conditions

$$D(1, 1) = d(1, 1) \quad (15)$$

$$D(k, 1) = d(k, 1) + D(k-1, 1) \text{ for } k = 2, \dots, 120 \quad (16)$$

$$D(1, l) = d(1, l) + D(1, l-1) \text{ for } l = 2, \dots, 120 \quad (17)$$

The DTW distance is the minimum cumulative cost along a valid alignment path α

$$DTW(P_c, M_c) = \min_{\alpha} \sum_{(k,l) \in \alpha} d(k, l) = D(K, L) \quad (18)$$

Here, $\alpha = [(k_1, l_1), (k_2, l_2), \dots, (k_{120}, l_{120})]$ denotes a warping path through the matrix D , matching the k -th point of the polymer curve to the l -th point of the metal curve. A path α is valid if it begins at (1,1) and ends at (K, L), $k_{i+1} > k_i$ and $l_{i+1} > l_i$, and $(k_{i+1} - k_i, l_{i+1} - l_i) \in [(1,0), (0,1), (1,1)]$. The average

DTW distance between a polymer material with multiple curves (P_1, P_2, \dots, P_Q) and a metal material with multiple curves (M_1, M_2, \dots, M_R) is

$$AvgDTW = \frac{1}{Q} \sum_{q=1}^Q \frac{1}{R} \sum_{r=1}^R DTW(P_q, M_r) \quad (19)$$

Finally, after obtaining the average DTW distances between each polymer and the target metal, we can rank them by numerical size and select one polymer with the smallest DTW distance as the source domain dataset.

2.3 Experimental design and data description

To comprehensively demonstrate the effectiveness of the DTW-TL framework, several additively manufactured polymers and metals that are fabricated by different kinds of AM techniques are selected. Specifically, there are four source polymer datasets and three target metal datasets. Nylon, PLA, and CF-ABS samples are fabricated by FFF and Resin samples are fabricated by DLP. AlSi10Mg and Ti6Al4V samples are fabricated by FFF, and carbon steel samples are fabricated by WAAM. As summarized in Table 1, four source polymers and three target metals span a broad spectrum of mechanical behaviors. Source polymers differ not only in strength and elongation but in underlying chemistry and molecular microstructure. Nylon, a semi-crystalline polyamide that can achieve over 200% elongation owing to its long, hydrogen-bonded chains that readily reorient under load and its interlayer fusion during filament melting. PLA, by contrast, is an amorphous polyester whose higher glass transition and limited chain mobility produce a modest 6% elongation and an ultimate tensile strength of 53 MPa. CF-ABS blends short carbon fibers into an ABS matrix, the rigid fibers raise stiffness (77 MPa) but act as crack initiation sites, restricting the elongation to just 1.25%. The Resin samples yields moderate ductility (10%) and an ultimate tensile strength of 48 MPa due to its lightly cross-linked network.

Table 1. Source polymers and target metals.

	Material	AM technique	Ultimate tensile strength (MPa)	Elongation at break
Source domain (polymer)	Nylon	FFF	34	210%
	PLA		53	6%
	CF-ABS		77	1.25%
	Resin	DLP	48	10%
Target domain (metal)	AlSi10Mg	L-PBF	460	6%
	Ti6Al4V		1060	15%
	Carbon steel	WAAM	648	24%

For target metals, AlSi10Mg samples that are fabricated by L-PBF solidify under extreme cooling rates, forming a fine cellular α -Al matrix interspersed with brittle eutectic Si networks and residual micro-porosity. This microstructure delivers the lowest tensile strength and restricts elongation to 6% because the hard, interconnected Si phase and layer boundary defects act as crack initiation sites. In contrast, Ti6Al4V samples fabricated by L-PBF develops a mixed $\alpha + \beta$ structure with high lattice friction and fine prior β grain boundaries. These features confer very high strength while its dual phase nature still permits dislocation slip for a reasonable 15% elongation. For carbon steel samples fabricated by WAAM, however, cools far more slowly, yielding a coarse ferrite pearlite microstructure with larger, equiaxed grains and fewer interlayer discontinuities. Although its ultimate tensile strength is only intermediate of 648 MPa compared to the other metals, the coarse ferrite pearlite microstructure of carbon steel accommodates extensive plastic deformation, resulting in the highest ductility of the three metals.

For the Nylon, PLA, and CF-ABS samples, an FFF-based Ultimaker S3 printer (Ultimaker, Netherlands) with a 250 μm nozzle diameter was used. Nylon (Ultimaker, Netherlands), PLA (Pro Series, MatterHackers, USA), and CF-ABS (Push Plastic, USA) filaments all had a 2.85 mm diameter. For Resin samples, a DLP-based FlashForge Foto printer (FlashForge, China) with a standard photopolymer resin was used. All polymer samples were in accordance with ASTM D638 Type V [31]. After fabrication, we performed uniaxial tensile tests on a universal test frame (AGS-X Series, Shimadzu, Japan) to quantitatively characterize the stress-strain behaviors. The load capacity of the test frame was 10 kN. The test speed and sampling frequency were 2 mm/min and 10 Hz, respectively. A full factorial design of experiments (DOE) was developed to collect experimental data with varying parameters of each material. Table 2 and Table A.1 show the details of DOE: each material involved two process parameters, and each parameter was set at five numerical levels, resulting in a total of 25 samples per polymer dataset.

Table 2. Design of experiments of the polymers and metals.

Domain	Material	Dataset	Parameter	Number of samples	Standard
Source domain (polymer)	Nylon	-	Print speed (mm/s) Print temperature ($^{\circ}\text{C}$)	25	ASTM D638
	PLA	-	Print speed (mm/s) Print temperature ($^{\circ}\text{C}$)	25	
	CF-ABS	-	Print speed (mm/s) Print temperature ($^{\circ}\text{C}$)	25	
	Resin	-	UV exposure time (s) Post processing time (min)	25	
Target domain (metal)	AlSi10Mg	1	Hatch spacing = 0.1 mm Laser power (W) Scanning speed (mm/s)	32	ASTM E8/E8M
		2	Hatch spacing = 0.15 mm Laser power (W) Scanning speed (mm/s)	28	
	Ti6Al4V	1	Flat geometry Laser power (W) Scanning speed (mm/s)	42	
		2	Round geometry Laser power (W) Scanning speed (mm/s)	42	
	Carbon steel	-	Build angle ($^{\circ}$) Nozzle angle ($^{\circ}$)	18	DIN 50125

For the AlSi10Mg dataset, it was published by the Pennsylvania State University [32], all samples were in accordance with ASTM E8/E8M [33] and fabricated with a 3D Systems ProX DMP 320 L-PBF system machine (3D System, Inc, United States) using gas atomized LaserForm AlSi10Mg (A) AlSi10Mg metallic powder (3D System, Inc, United States). Table 1 and Table B.1 show the DOE, 60 samples were fabricated with varying laser power, scanning speed, and hatch spacing. Specifically, the samples fabricated with hatch spacing of 0.1 mm are defined as the AlSi10Mg dataset 1 (size of the dataset is 32), the remaining samples fabricated with hatch spacing of 0.15 mm are defined as the AlSi10Mg dataset 2 (size of the dataset is 28).

For the Ti6Al4V dataset, it was also published by the Pennsylvania State University [34], all samples were fabricated accordance with the same ASTM standard and L-PBF system using LaserForm Ti Gr23(A) Ti-6Al-4V powder (3D Systems, Inc, United States). Table 2 and Table B.2 show the DOE, 84 samples were fabricated with varying laser power, scanning speed, and geometry. Specifically, the samples fabricated with flat geometry are defined as the Ti-6Al-4V dataset 1 (size of the dataset is 42), the remaining samples

fabricated with round geometry are defined as the Ti-6Al-4V dataset 2 (size of the dataset is 42). After fabrication, uniaxial tensile tests were performed for the metal samples by an electromechanical load frame (Criterion Model 45, MTS Systems, Inc., United States) with maximum load of 10 kN and a quasi-static strain rate of 3×10^{-4} /s.

Table 3. Divisions of the dataset.

	Case	Training dataset	Test dataset	No. of data points	
				Training dataset	Test dataset
Vanilla LSTM model	1	AlSi10Mg dataset 1: Sample 1 and 20	Remaining 30 samples in AlSi10Mg dataset 1	951	14,956
	2	AlSi10Mg dataset 2: Sample 33 and 47	Remaining 26 samples in AlSi10Mg dataset2	443	10,240
	3	Ti6Al4V dataset 1: Sample 27 and 38	Remaining 40 samples in Ti6Al4V dataset 1	983	25,898
	4	Ti6Al4V dataset 2: Sample 69 and 80	Remaining 40 samples in Ti6Al4V dataset 2	1,778	43,180
	5	Carbon steel dataset: Sample 1 and 2	Remaining 16 samples in carbon steel dataset	473	3,564
TL model using all four polymers as the source domain	Case	Source domain	Target domain		
			Training dataset	Test dataset	
	1	Nylon, PLA, CF-ABS, and Resin	AlSi10Mg dataset 1: Sample 1 and 20	Remaining 30 samples in AlSi10Mg dataset 1	
	2	Nylon, PLA, CF-ABS, and Resin	AlSi10Mg dataset 2: Sample 33 and 47	Remaining 26 samples in AlSi10Mg dataset 2	
	3	Nylon, PLA, CF-ABS, and Resin	Ti6Al4V dataset 1: Sample 27 and 38	Remaining 40 samples in Ti6Al4V dataset 1	
	4	Nylon, PLA, CF-ABS, and Resin	Ti6Al4V dataset 2: Sample 69 and 80	Remaining 40 samples in Ti6Al4V dataset 2	
5	Nylon, PLA, CF-ABS, and Resin	Carbon steel dataset: Sample 1 and 2	Remaining 16 samples in carbon steel dataset		
DTW-TL model using only one polymer as the source domain	Case	Source domain (based on DTW distance to select one)	Target domain		
			Training dataset	Test dataset	
	1	Nylon, or PLA, or CF-ABS, or Resin	AlSi10Mg dataset 1: Sample 1 and 20	Remaining 30 samples in AlSi10Mg dataset 1	
	2	Nylon, or PLA, or CF-ABS, or Resin	AlSi10Mg dataset 2: Sample 33 and 47	Remaining 26 samples in AlSi10Mg dataset 2	
	3	Nylon, or PLA, or CF-ABS, or Resin	Ti6Al4V dataset 1: Sample 27 and 38	Remaining 40 samples in Ti6Al4V dataset 1	
	4	Nylon, or PLA, or CF-ABS, or Resin	Ti6Al4V dataset 2: Sample 69 and 80	Remaining 40 samples in Ti6Al4V dataset 2	
5	Nylon, or PLA, or CF-ABS, or Resin	Carbon steel dataset: Sample 1 and 2	Remaining 16 samples in carbon steel dataset		

For the carbon steel dataset, it was published by the ETH Zurich [35]. The experimental robotic welding setup was comprised of an ABB IRB 4600/40 robot, a Fronius TPS 500i Pulse power source, and a Fronius 60i Robacta Drive Cold Metal Transfer (CMT) torch with a 22° neck. The standard DIN 50125 was considered for the design of the test specimens. Table 2 and Table B.3 show the DOE of carbon steel dataset.

A total of 18 samples were fabricated with varying build angles and nozzle angles. After fabrication, uniaxial tensile tests were performed on a Zwick universal testing machine able to apply loads up to 200 kN. The tests were carried out in a conditioned room at 23 °C and 50% relative humidity. The specimens were clamped on each side over a length of 40 mm. The load was applied displacement-controlled with a constant displacement rate of 0.01 mm/s.

Table 3 provides the divisions of the dataset for vanilla LSTM model, TL model using all four polymers as the source domain, and DTW-TL model using only one polymer as the source domain. In the vanilla LSTM model, only two specific samples are selected for training, as their parameters both represent either the maximum or minimum values in the entire DOE. This selection ensures that training dataset captures the extreme boundary conditions, allowing the model to learn the most distinct mechanical behaviors with minimum amount of data. The test dataset consists of the remaining samples within the same dataset to evaluate model performance. Table 3 also highlights the significant difference between the number of data points in training and test datasets, demonstrating the effectiveness of the framework in achieving good prediction results with minimal training data. Compared with the vanilla LSTM model, the TL model using all four polymers as the source domain leverages multiple source domain datasets for additional pre-training. All source domain datasets are first concatenated into a unified dataset and then randomly shuffled before pretraining. And the divisions of training and test datasets in the target domain are the same as the ones in the vanilla LSTM model. For the DTW-TL model using only one polymer as the source domain, only one polymer dataset is selected to form the source domain based on the DTW distance. And the same division strategy for the target domain is applied as the TL model using all four polymers as the source domain.

3. Results and discussions

3.1 Mechanical behaviors of additively manufactured polymers and metals

Fig. 3 illustrates the stress-strain curves of samples fabricated with varying parameters for seven different materials, including four polymers (i.e., Nylon, PLA, CF-ABS, and Resin) and three metals (i.e., AlSi10Mg, Ti6Al4V, and carbon steel). Each material subplot highlights the influence of process parameters on stress-strain behaviors.

Four polymers exhibit distinct mechanical behaviors according to their stress-strain curves, including stiffness, strength, and ductility. Nylon samples (Fig. 3a) exhibit abrupt yield drop followed by oscillatory softening and the longest post-yield plateau region among polymers. PLA (Fig. 3b) and CF-ABS samples (Fig. 3c) both display immediate strain hardening upon yielding. And Resin samples (Fig. 3d) form smooth, continuous post-yield plateau region. These distinct post-yield behaviors reflect their underlying chemistry and molecular architecture. Nylon is a semi-crystalline polyamide whose rigid crystalline lamellae are interspersed with an amorphous matrix. After yielding, its hydrogen-bonded chains uncoil and slide extensively, allowing distributed plastic flow and the longest post-yield plateau of the group. Layer-to-layer interdiffusion in FFF printing further smooths stress gradients, reinforcing its ductility. PLA is a highly stereoregular, partially crystalline polyester. Its uniform chain packing gives a high elastic modulus and sharp yield, but limited amorphous content and weak inter-chain friction cause rapid fracture just beyond yield, resulting in very low elongation. CF-ABS combines an amorphous ABS matrix with stiff carbon-fiber reinforcements. The fibers raise the initial elastic modulus and postpone macro-crack initiation, producing immediate work-hardening as the polymer yields. Resin is a densely crosslinked photopolymer network. Upon yielding, covalent network bonds break and reform under load, producing a smooth, continuous plateau as energy is dissipated through distributed shear banding rather than localized cracks, ultimately failing in a brittle manner.

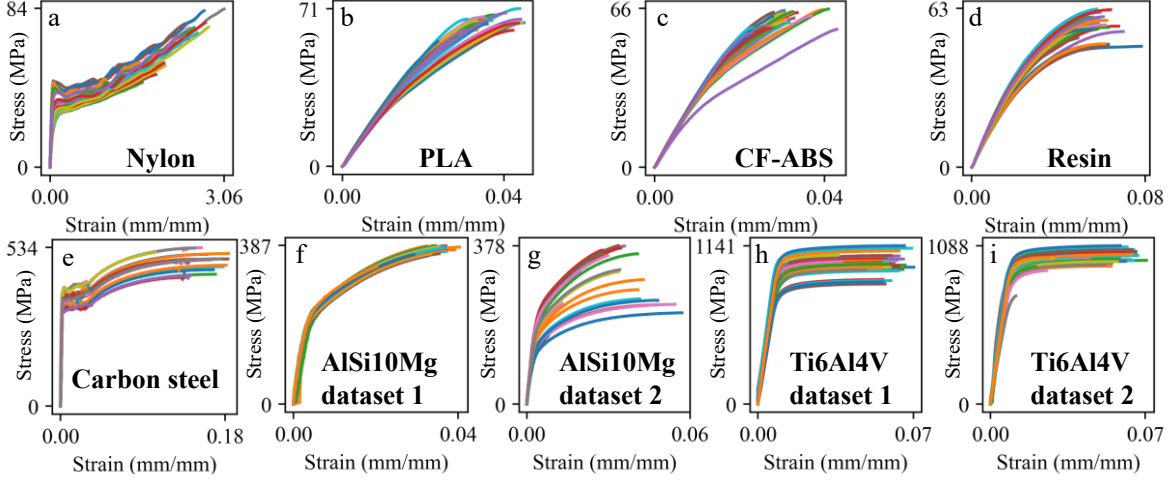


Fig. 3. Stress-strain curves of the samples fabricated with polymers or metals. Polymers: (a) Nylon, (b) PLA, and (c) CF-ABS fabricated by FFF, (d) Resin fabricated by DLP. Metals: (e) carbon steel fabricated by wire arc, (f) AlSi10Mg dataset 1, (g) AlSi10Mg dataset 2, (h) Ti6Al4V dataset 1, and (i) Ti6Al4V dataset 2 fabricated by L-PBF.

Although metals display significantly higher strength and stiffness than polymers, metals and polymers have several similar mechanical behaviors, especially after yield. Yield drops and subsequent plateau regions of carbon steel samples (Fig. 3e) that driven by dislocation unlocking and band propagation in its ferrite–pearlite microstructure are closely similar to Nylon samples. In contrast, both AlSi10Mg (Fig. 3f-g) and Ti6Al4V samples (Fig. 3h-i) exhibit smooth, monotonic work-hardening, which is driven by uniform slip in the α -Al matrix with Si precipitates of AlSi10Mg samples and progressive dislocation build-up in the $\alpha + \beta$ lamellae of Ti6Al4V samples. This behavior mirrors the continuous post-yield plateau region of Resin samples. These similarities of mechanical behaviors between polymers and metals are precisely what the proposed DTW-TL framework utilizes, identifying the closest match between polymers and metals (i.e., Resin with AlSi10Mg and Ti6Al4V, Nylon with carbon steel) to achieve the most accurate stress-strain predictions of additively manufactured metals.

3.2 Correlation between dynamic time warping distance and predictive performance

Table 4 demonstrates that for each target metal, the source polymer with the smallest DTW distance also yields the best predictive performance. For AlSi10Mg datasets 1 and 2, when Resin is selected as the source domain dataset, their stress-strain curves have the closest alignment (DTW distances are 0.085 and 0.055) and the DTW-TL model achieves the best predictive performance (MAPEs are 7.01% and 17.12%), outperforming Nylon, PLA, and CF-ABS. For Ti6Al4V datasets 1 and 2, when Resin is selected as the source domain dataset, their stress-strain curves have the closest alignment (DTW distances are 0.073 and 0.061) and the DTW-TL model achieves the best predictive performance (MAPEs are 11.95% and 13.09%). For carbon steel, Nylon is the most similar source with DTW distance of 0.586 and achieves the lowest MAPE of 18.23%. As mentioned in Section 3.1, the closest matches of mechanical behaviors between polymers and metals are Resin with AlSi10Mg and Ti6Al4V, Nylon with carbon steel, which are accurately identified by the proposed DTW process. Meanwhile, high Pearson correlation coefficients between DTW distances and MAPEs demonstrate that DTW distance is a reliable distance metric to correlate similarity of stress-strain behaviors and predictive performance of TL model.

Moreover, Fig. 4 further visualizes the normalized and interpolated stress-strain curves of four source polymers and three target metals. Before applying DTW, each curve is scaled by its maximum stress and strain and resampled onto a strain grid. This pre-processing removes differences in absolute magnitude and uneven data density, ensuring that DTW compares the curve shapes rather than trivial scale effects. Consequently, in Fig. 4a and 4b, the Resin curve aligns most closely with those of AlSi10Mg and Ti6Al4V.

And in Fig. 4c, the Nylon curve best matches the carbon steel curve, confirming that normalized and interpolated curves can truly reflect the similarity between stress-strain curves polymers and metals.

Table 4. DTW distances and MAPEs when transferring from different source polymers to target metals.

Target domain: metal	Source domain: polymer	DTW distance	MAPE	Pearson correlation coefficient between DTW distance and MAPE
AlSi10Mg dataset 1	(Nylon, PLA, CF-ABS, Resin)	(0.173, 0.100, 0.097, 0.085)	(42.07%, 9.80%, 9.49%, 7.01%)	0.996
AlSi10Mg dataset 2	(Nylon, PLA, CF-ABS, Resin)	(0.250, 0.063, 0.062, 0.055)	(35.81%, 33.39%, 30.13%, 17.12%)	0.567
Ti6Al4V dataset 1	(Nylon, PLA, CF-ABS, Resin)	(0.280, 0.080, 0.079, 0.073)	(54.76%, 16.39%, 16.24%, 11.95%)	0.997
Ti6Al4V dataset 2	(Nylon, PLA, CF-ABS, Resin)	(0.286, 0.065, 0.064, 0.061)	(30.81%, 17.11%, 16.49%, 13.09%)	0.977
Carbon steel	(PLA, CF-ABS, Resin, Nylon)	(1.027, 0.999, 0.882, 0.586)	(43.68%, 32.45%, 28.44%, 18.23%)	0.908

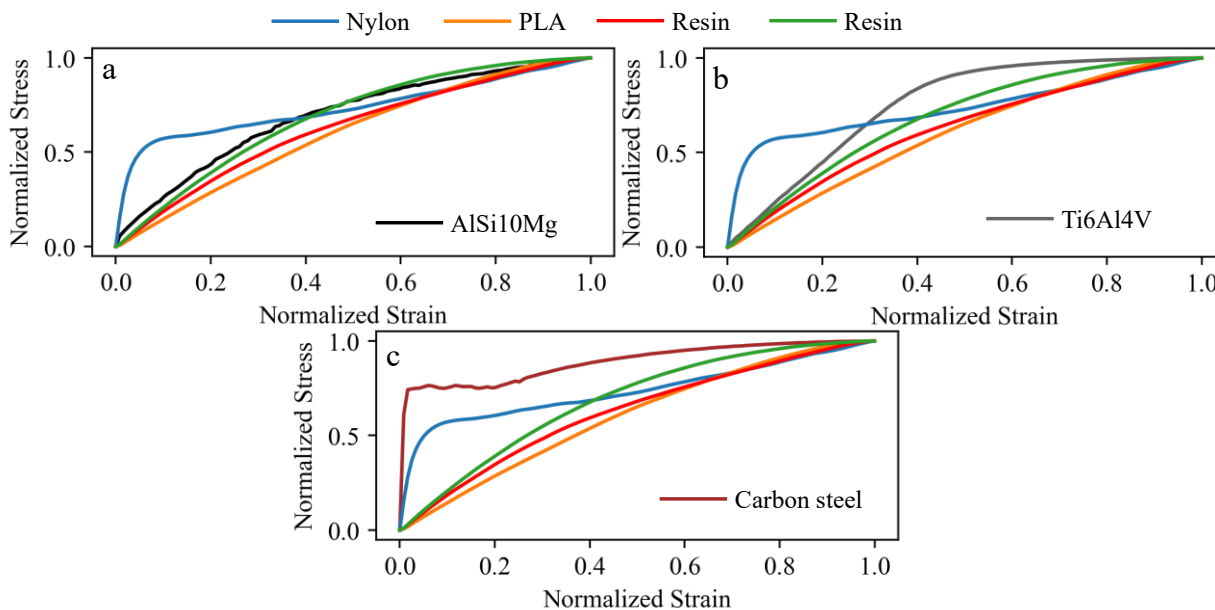


Fig. 4. Normalized and interpolated stress-strain curves of four source polymers (i.e., Nylon, PLA, CF-ABS, and Resin) compared with (a) AlSi10Mg, (b) Ti6Al4V, and (c) carbon steel.

3.3 Predicted stress-strain curves of AlSi10Mg

Table 5 presents the MAPEs for predicting the stress-strain curves of AlSi10Mg samples across different models. For the vanilla LSTM model without TL, the MAPEs are relatively high, which are 13.31% for AlSi10Mg dataset 1 and 35.50% for AlSi10Mg dataset 2. After incorporating TL that uses all four polymers as the source domain, it shows improvement of predictive performance. However, when using DTW to

select one polymer material with the minimum DTW distance as the source domain, the predictive performance is continuously improved. As shown in Table 5, when the Resin dataset is selected as the source domain, the model achieves the lowest MAPEs of 6.00% for dataset 1 and 18.51% for dataset 2. Moreover, the marked difference in MAPEs between AlSi10Mg datasets is due to number of data points in the training dataset and variability of stress-strain curves. AlSi10Mg dataset 2 contains only 443 data points in the training dataset, less than half of the 951 data points in AlSi10Mg dataset 1. And stress-strain curves in AlSi10Mg dataset 2 (Fig. 3g) display substantially greater scatter than stress-strain curves in AlSi10Mg dataset 1 (Fig. 3f). This reduction in training examples, combined with increased variability in mechanical behaviors, raising the average MAPEs for all models of AlSi10Mg dataset 2.

Table 5. Prediction MAPEs of AlSi10Mg samples.

Target domain	AlSi10Mg dataset 1	AlSi10Mg dataset 2
Vanilla LSTM model	No source domain pre-training	
	13.31%	35.50%
TL model using all four polymers as the source domain	Source domain consists of Nylon, PLA, CF-ABS, and Resin	
	8.96%	25.04%
DTW-TL model using only one polymer as the source domain	Source domain only consists of Resin	
	7.01%	17.12%

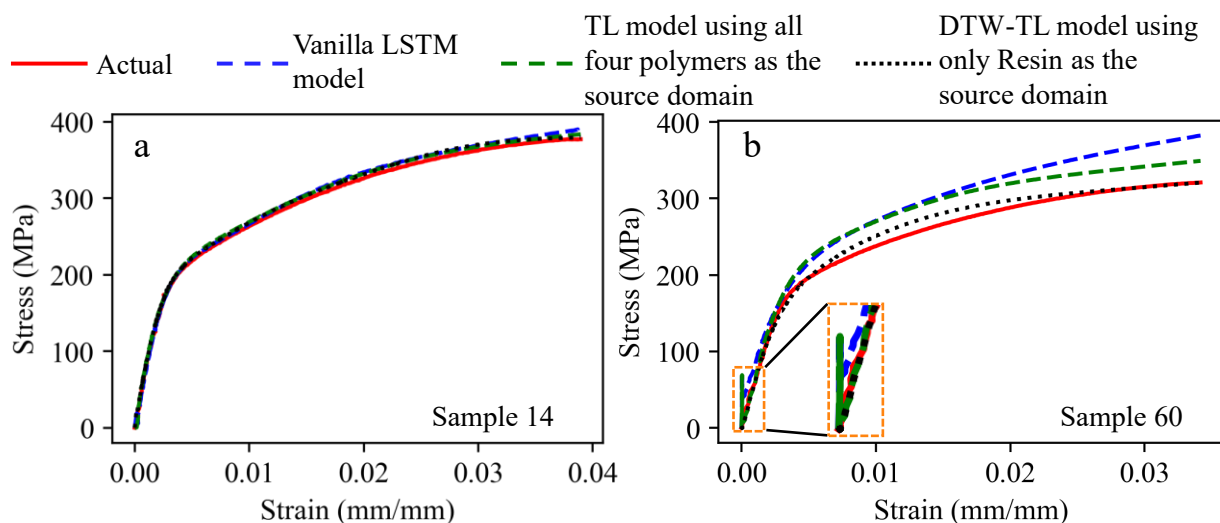


Fig. 5. Actual versus predicted stress-strain curves of AlSi10Mg samples using different models. (a) sample 14 in AlSi10Mg dataset 1, (b) sample 60 in AlSi10Mg dataset 2.

Fig. 5 illustrates the comparison between actual stress-strain curves of AlSi10Mg samples and their predicted ones using different models: vanilla LSTM model, TL model using all four polymers as the source domain, and DTW-TL model only using Resin as the source domain. For AlSi10Mg dataset 1, as shown in Fig. 5a, the predictions of different models are relatively accurate. However, in the region before failure, the curve predicted by DTW-TL model that only uses Resin as the source domain outperforms other models by closely following the actual stress-strain trend. For AlSi10Mg dataset 2, as shown in Fig. 5b, a more noticeable difference in predictive performance between the different models is observed. For example, the curve predicted by TL model using all four polymers as the source domain introduces the peaks in the elastic region which do not reflect realistic mechanical behavior. In the plastic region, the curve predicted by DTW-TL model also effectively captures the actual stress-strain trend to achieve the most accurate predictions, especially higher strains, where the other two models show significant overpredictions.

Fig. 6 illustrates the prediction results of TL models for predicting the stress-strain curves of AlSi10Mg samples when different polymer materials are used as the source domain. The red dashed line represents the ideal case between actual and predicted stress, providing a benchmark for model performance. Average MAPEs of each sample are presented as violin plots, highlighting the variability in predictive performance. For AlSi10Mg dataset 1, as shown in Fig. 6a, the TL model pre-trains by Nylon exhibits the highest average MAPE, with a maximum value even reaching 361%. For the predictions of stress values above 200 MPa, the TL model pre-trains by Resin achieves higher predictive performance compared to the TL models pre-trains by PLA and CF-ABS, evidenced by significantly fewer data points deviating far from the red dashed line. For AlSi10Mg dataset 2, similar trends can be observed. The TL model pre-trains by Nylon or CF-ABS both exhibit the highest MAPE above 200%, followed by PLA at 97%, which indicate less accurate predictions compared to the Resin one, which achieves a relatively low MAPE range between 2% and 34%. For the predictions of stress values below 50 MPa, only TL model pre-trains by Resin achieves acceptable performance with minimal deviations points.

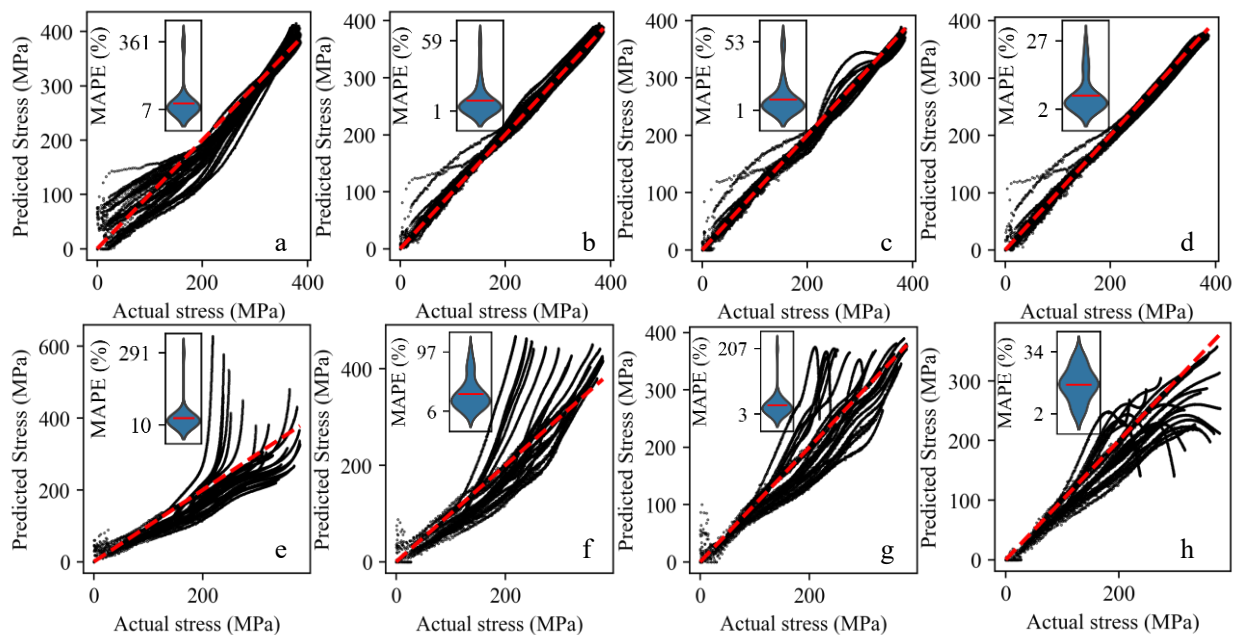


Fig. 6. Actual versus predicted stresses of AlSi10Mg samples using different polymer materials as the source domain. (a) Nylon, (b) PLA, (c) CF-ABS, and (d) Resin for AlSi10Mg dataset 1. (e) Nylon, (f) PLA, (g) CF-ABS, and (h) Resin for AlSi10Mg dataset 2.

3.4 Predicted stress-strain curves of Ti6Al4V

Table 6 summarizes the MAPEs for predicting the stress-strain curves of Ti6Al4V samples across different models. For the vanilla LSTM model without TL, the MAPEs are relatively high, reaching 14.33% for Ti6Al4V dataset 1 and 22.82% for Ti6Al4V dataset 2. When TL is applied and uses all four polymers as the source domain, the predictive performance even fails to improve, the MAPEs increase to 18.18% for Ti6Al4V dataset 1 and 30.20% for Ti6Al4V dataset 2. In contrast, integrating DTW to select the most relevant polymer as the source domain achieves notable improvements. When Resin dataset is selected as the source domain, the model achieves the lowest MAPEs of 11.95% for Ti6Al4V dataset 1 and 13.09% for Ti6Al4V dataset 2.

Fig. 7 compares the actual and predicted stress-strain curves of Ti6Al4V samples using different models: vanilla LSTM model, TL model using all four polymers as the source domain, and DTW-TL model only using Resin as the source domain. For prediction results of Ti6Al4V dataset 1 shown in Fig. 7a, TL model using all four polymers as the source domain predicts a noticeable peak at the beginning of the strain.

However, DTW-TL model that only uses Resin as the source domain performs the best, closely aligning with the actual curves. For predictions of Ti6Al4V dataset 2 shown in Fig. 7b, both vanilla LSTM model and TL model using all four polymers as the source domain introduce a peak at the beginning of the strain, but only DTW-TL model avoids the unrealistic increase followed by a decrease in stress. In the plastic region, DTW-TL model continues to outperform the other models by accurately capturing stress-strain trends, particularly at higher strains. Only DTW-TL model predicts the actual ultimate tensile strength at last. In contrast, the other two models significantly underpredict this mechanical property.

Table 6. Prediction MAPEs of the Ti6Al4V samples.

Target domain	Ti6Al4V dataset 1	Ti6Al4V dataset 2
Vanilla LSTM model	No source domain pre-training	
	14.33%	22.82%
TL model using all four polymers as the source domain	Source domain consists of Nylon, PLA, CF-ABS, and Resin	
	18.18%	30.20%
DTW-TL model using only one polymer as the source domain	Source domain consists of only Resin	
	11.95%	13.09%

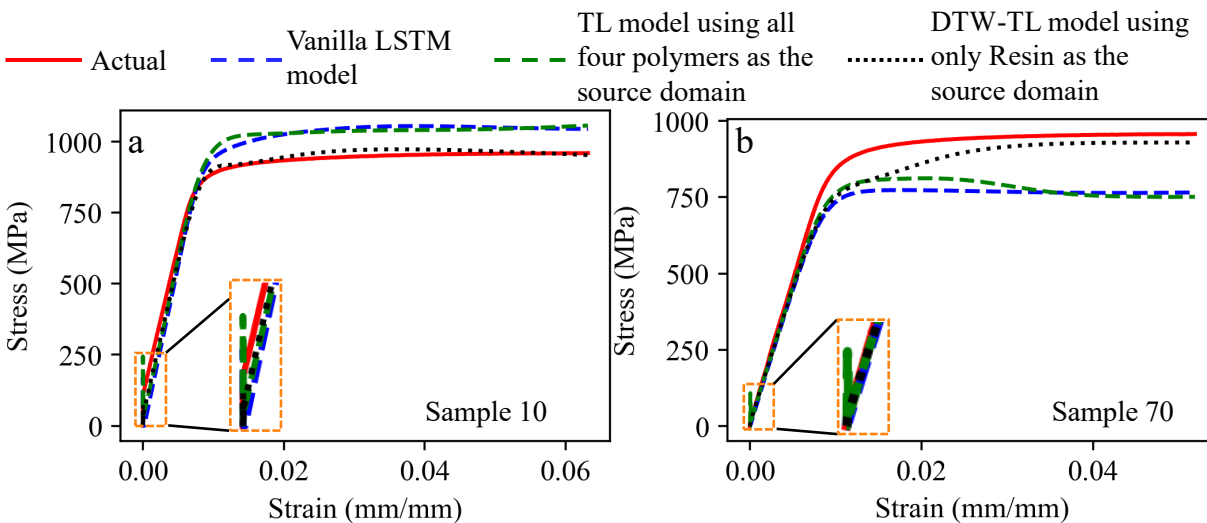


Fig. 7. Actual versus predicted stress-strain curves of Ti6Al4V samples using different models. (a) sample 10 in Ti6Al4V dataset 1, (b) sample 70 in Ti6Al4V dataset 2.

Fig. 8 illustrates the prediction results of TL models for predicting the stress-strain curves of Ti6Al4V samples when different polymer materials are used as the source domain. The red dashed line represents the ideal case, providing a benchmark for predictive performance. Average MAPEs of each sample are presented as violin plots, highlighting the variability in predictive performance. For Ti6Al4V dataset 1, predictions of the TL model pre-trains by Nylon (Fig. 8a) exhibit the highest average MAPE, with variability reaching up to 1000%. The scatter plot reveals that the predictions of the TL model pre-trains by Nylon show substantial deviations in the whole stress range, while the PLA one (Fig. 8b) performs poorly within 750 MPa to 1000 MPa. For the predictions of stress values below 50 MPa, when using Resin as the source domain (Fig. 8d), there are no significant deviation points, the predicted values do not exhibit extreme overpredictions, such as exceeding 100 MPa, which is observed in other models. For Ti6Al4V dataset 2, the trends are consistent with those observed in Ti6Al4V dataset 1. The TL model pre-trains by Nylon (Fig. 8e) or PLA (Fig. 8f) both show a larger range of MAPEs, demonstrating noticeable deviations across the entire stress range, failing to align with the red dashed line. Compared with the TL model pre-

trains by CF-ABS (Fig. 8g), the Resin one (Fig. 8h) better aligns the red line across the whole stress range, achieving the lowest MAPEs ranging from 4% to 26%.

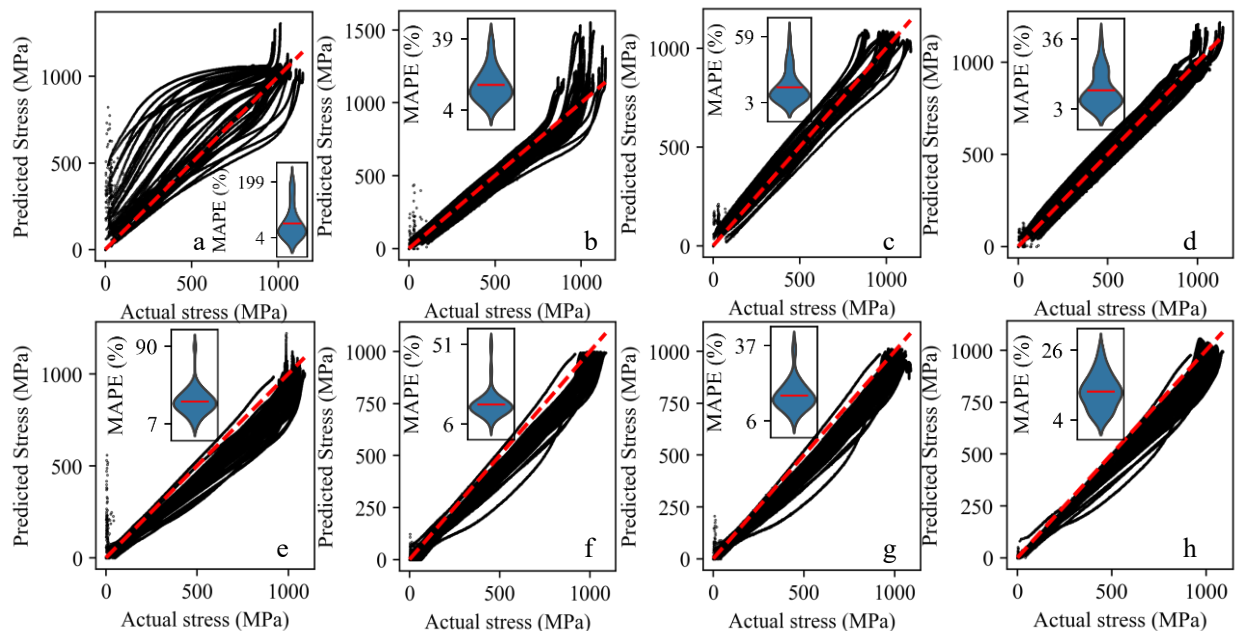


Fig. 8. Actual versus predicted stresses of Ti6Al4V samples using different polymer materials as the source domain. (a) Nylon, (b) PLA, (c) CF-ABS, and (d) Resin for Ti6Al4V dataset 1. (e) Nylon, (f) PLA, (g) CF-ABS, and (h) Resin for Ti6Al4V dataset 2.

3.5 Predicted stress-strain curves of carbon steel

Table 7 presents the MAPEs in predicting the stress-strain curves of carbon steel samples across different models. For the vanilla LSTM model without TL, it achieves a relatively high MAPE of 26.28%. After incorporating TL that uses all four polymers as the source domain, it shows improvement of predictive performance. However, when using DTW to select one polymer material with the minimum DTW distance as the source domain, the predictive performance is continuously improved. Specifically, when the source domain only contains Nylon dataset, the model achieves the lowest MAPEs of 18.23%.

Table 7. Prediction MAPEs of the carbon steel samples.

Target domain	Carbon steel
Vanilla LSTM model	No source domain pre-training
	26.28%
TL model using all four polymers as the source domain	Source domain consists of Nylon, PLA, CF-ABS, and Resin
	21.25%
DTW-TL model using only one polymer as the source domain	Source domain consists of only Nylon
	18.23%

Fig. 9 illustrates the comparison between actual stress-strain curves of carbon steel samples and predicted ones using different models: vanilla LSTM model, TL model using all four polymers as the source domain, and DTW-TL model only using Nylon as the source domain. Within the region before yield, the predictions of different models are relatively accurate. However, the curve predicted by DTW-TL that only uses Nylon as the source domain outperforms other models by closely following the actual stress-strain trend within the post-yield region. In contrast, vanilla LSTM model and TL model using all four polymers as the source domain show overpredictions.

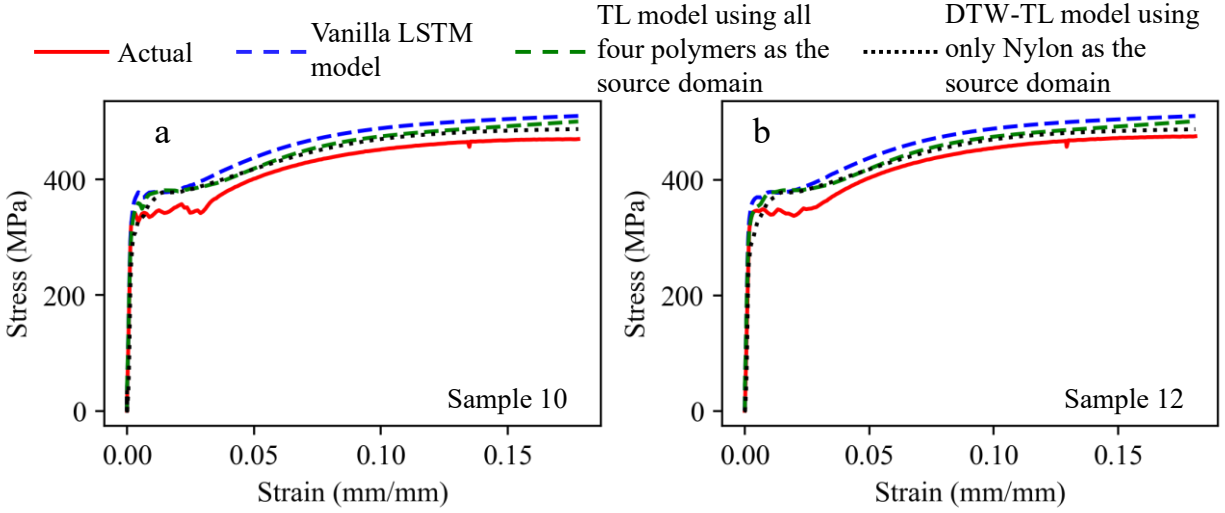


Fig. 9. Actual versus predicted stress-strain curves of carbon steel samples using different models. (a) sample 10 and (b) sample 12 in carbon steel dataset.

Fig. 10 illustrates the prediction results of TL models for predicting the stress-strain curves of carbon steel samples when different polymer materials are used as the source domain. The red dashed line represents the ideal case, providing a benchmark for predictive performance. Average MAPEs of each sample are presented as violin plots, highlighting the variability in predictive performance. When using PLA (Fig. 10a) or CF-ABS (Fig. 10b) as the source domain, the model exhibits noticeable scatters within the whole stress range, yielding a relatively high MAPE range from 15% to 106% and 15% to 73%. Pre-training on Resin (Fig. 10c) improves alignment with the red line, but the prediction results still show underpredictions or overpredictions. In contrast, the TL model pre-trains on Nylon (Fig. 10d) performs best, the scatters are more cluster around the ideal red line. And its violin plot reflects both the lowest median MAPE and the narrowest variability from 8% to 34%.

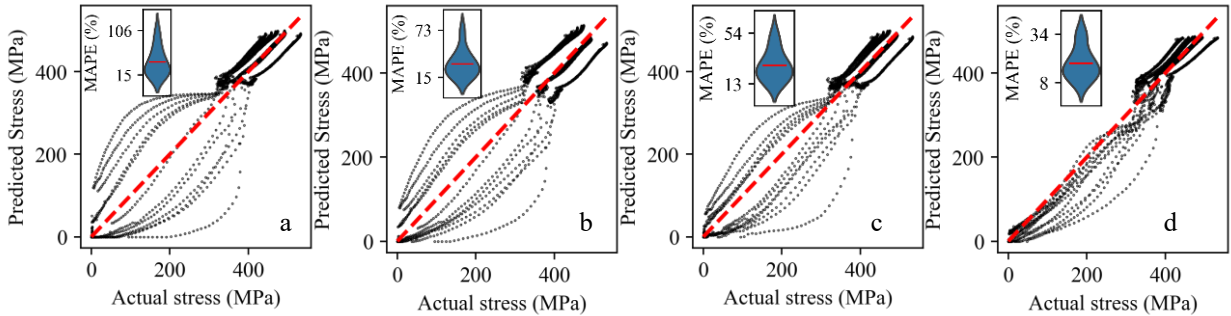


Fig. 10. Actual versus predicted stresses of carbon steel samples using different polymer materials as the source domain. (a) PLA, (b) CF-ABS, (c) Resin, and (d) Nylon.

3.6 Predictive performance comparison

Table 8 presents a comparison of the average predictive performance across all target metal datasets, including AlSi10Mg dataset 1, AlSi10Mg dataset 2, Ti6Al4V dataset 1, Ti6Al4V dataset 2, and carbon steel dataset. Surprisingly, the vanilla LSTM model, which involves no TL, achieves lower MAPE of 20.52% compared to TL model using all four polymers as the source domain. This suggests that without proper domain alignment, simply increasing the size and diversity of the source domain data can negatively impact predictive performance. In contrast, DTW-TL model that only use Resin or Nylon as the source domain demonstrates superior predictive performance, achieving the best predictive performance with a MAPE of

12.41%, a RMSE of 63.75, and a R^2 of 0.96, despite utilizing a significantly smaller source domain dataset of only 3000 data points. This result highlights the importance of effective domain alignment through DTW, which ensures that the selected source domain closely matches the target domain, thereby achieving higher predictive performance with fewer pre-training data in the source domain.

Table 8. Comparison of the average predictive performance.

	MAPE	RMSE	R2	No. of data points in source domain dataset
Vanilla LSTM model	No source domain pre-training			
	20.52%	81.55	0.94	0
TL model using all four polymers as the source domain	Source domain consists of Nylon, PLA, CF-ABS, and Resin			
	22.92%	74.45	0.94	12,000
DTW-TL model using only one polymer as the source domain	Source domain consists of only Nylon or Resin			
	12.41%	63.75	0.96	3,000

4. Conclusions

A novel DTW-TL framework for AM part qualification was developed to predict the stress-strain behaviors of additively manufactured metals by transferring the knowledge from low-cost additively manufactured polymers. DTW was integrated into the framework to select only one source polymer which is the most relevant to the target metal. The framework was demonstrated on three target metals under tensile loads, including AlSi10Mg, Ti6Al4V, and carbon steel datasets. When target domain contained AlSi10Mg or Ti6Al4V dataset, the Resin dataset was selected as the source domain because DTW process identified these two materials both had continuous post-yield plateau region. When carbon steel dataset was regarded as the target domain, the Resin dataset was selected as the source domain because DTW process identified these two materials both had yield drops and subsequent plateau regions. Experimental results showed that DTW-TL model using only one polymer dataset as the source domain achieved the lowest average MAPE of 12.41%, lowest RMSE of 63.75, and highest R^2 of 0.96 across three target metal datasets, respectively, outperforming vanilla LSTM model without TL and TL model using all four polymer datasets as the source domain. Notably, this performance improvement was achieved using a substantially smaller source training dataset with 3,000 data points compared to the initial source domain dataset with 12,000 data points. In addition, pre-training the TL model on all four polymer datasets did not improve predictive performance but resulted in a higher MAPE of 22.92% compared to the vanilla LSTM model. These results highlighted the effectiveness of DTW-TL framework in refining the source domain selection process, ensuring optimal knowledge transfer from polymers to metals. The proposed framework provides a systematic and efficient method for improving predictive performance of metal stress-strain behaviors while reducing data collection efforts and related costs, making it a valuable contribution to AM part qualification.

Acknowledgments

This research is sponsored by the Defense Advanced Research Projects Agency. The content of the information does not necessarily reflect the position or the policy of the Government. No official endorsement should be inferred. We would also like to thank Dr. Qingyang Liu for collecting the raw data of polymer datasets.

Data Availability Statement

The dataset generated and supporting the findings of this article are available upon reasonable request from the corresponding author.

Appendix A. DOE of additively manufactured polymer samples

Table A.1 DOE of Nylon, PLA, and CF-ABS samples.

Nylon			PLA			CF-ABS		
Sample ID	Print temperature (°C)	Print speed (mm/s)	Sample ID	Print temperature (°C)	Print speed (mm/s)	Sample ID	Print temperature (°C)	Print speed (mm/s)
1	220	10	1	180	10	1	200	10
2	220	20	2	180	30	2	200	30
3	220	30	3	180	50	3	200	50
4	220	40	4	180	70	4	200	70
5	220	50	5	180	90	5	200	90
6	230	10	6	200	10	6	220	10
7	230	20	7	200	30	7	220	30
8	230	30	8	200	50	8	220	50
9	230	40	9	200	70	9	220	70
10	230	50	10	200	90	10	220	90
11	240	10	11	220	10	11	240	10
12	240	20	12	220	30	12	240	30
13	240	30	13	220	50	13	240	50
14	240	40	14	220	70	14	240	70
15	240	50	15	220	90	15	240	90
16	250	10	16	240	10	16	260	10
17	250	20	17	240	30	17	260	30
18	250	30	18	240	50	18	260	50
19	250	40	19	240	70	19	260	70
20	250	50	20	240	90	20	260	90
21	260	10	21	260	10	21	280	10
22	260	20	22	260	30	22	280	30
23	260	30	23	260	50	23	280	50
24	260	40	24	260	70	24	280	70
25	260	50	25	260	90	25	280	90

Table A.1 DOE of Resin samples.

Sample ID	UV exposure time (s)	Post processing time (min)
1	2	2
2	2	4
3	2	6
4	2	8
5	2	10
6	2.5	2
7	2.5	4
8	2.5	6
9	2.5	8
10	2.5	10
11	3	2
12	3	4
13	3	6
14	3	8

15	3	10
16	3.5	2
17	3.5	4
18	3.5	6
19	3.5	8
20	3.5	10
21	4	2
22	4	4
23	4	6
24	4	8
25	4	10

Appendix B. DOE of additively manufactured metal samples

Table B.1 DOE of AlSi10Mg samples.

Dataset 1: hatch spacing = 0.1mm			Dataset 2: hatch spacing = 0.15mm		
Sample ID	Laser power (W)	Scanning speed (mm/s)	Sample ID	Laser power (W)	Scanning speed (mm/s)
1	60	250	33	60	250
2	160	250	34	160	250
3	160	800	35	160	800
4	160	1350	36	260	250
5	260	250	37	260	800
6	260	800	38	260	1350
7	260	1350	39	360	250
8	260	1900	40	360	800
9	360	250	41	360	1350
10	360	800	42	360	1900
11	360	1350	43	460	250
12	360	1900	44	460	800
13	360	2450	45	460	1350
14	360	3000	46	460	1900
15	460	250	47	460	2450
16	460	800	48	110	250
17	460	1350	49	110	500
18	460	1900	50	160	500
19	460	2450	51	260	500
20	460	3000	52	360	500
21	110	250	53	460	500
22	210	250	54	210	250
23	60	500	55	210	500
24	110	500	56	210	800
25	160	500	57	210	1100
26	210	500	58	260	1100
27	260	500	59	360	1100
28	360	500	60	460	1100
29	460	500			
30	110	800			
31	210	800			
32	210	1350			

Table B.2 DOE of Ti6Al4V samples.

Dataset 1: flat geometry			Dataset 2: round geometry		
Sample ID	Laser power (W)	Scanning speed (mm/s)	Sample ID	Laser power (W)	Scanning speed (mm/s)
1	275	800	43	275	800
2	275	760	44	275	760
3	275	720	45	275	720
4	275	680	46	275	680
5	275	640	47	275	640
6	275	600	48	275	600
7	275	840	49	275	840
8	275	880	50	275	880
9	275	920	51	275	920
10	275	960	52	275	960
11	275	1000	53	275	1000
12	175	800	54	175	800
13	195	800	55	195	800
14	215	800	56	215	800
15	235	800	57	235	800
16	255	800	58	255	800
17	295	800	59	295	800
18	315	800	60	315	800
19	335	800	61	335	800
20	355	800	62	355	800
21	375	800	63	375	800
22	135	400	64	135	400
23	205	600	65	205	600
24	345	1000	66	345	1000
25	415	1200	67	415	1200
26	485	1400	68	485	1400
27	500	1480	69	500	1480
28	155	400	70	155	400
29	235	600	71	235	600
30	395	1000	72	395	1000
31	475	1200	73	475	1200
32	500	1290	74	500	1290
33	115	400	75	115	400
34	175	600	76	175	600
35	295	1000	77	295	1000
36	355	1200	78	355	1200
37	475	1600	79	475	1600
38	75	400	80	75	400
39	115	600	81	115	600
40	195	1000	82	195	1000
41	235	1200	83	235	1200
42	315	1600	84	315	1600

Table B.3 DOE of carbon steel samples.

Sample ID	Build angle (°)	Nozzle angle (°)
-----------	-----------------	------------------

1	0	0
2	0	0
3	0	0
4	0	22.5
5	0	22.5
6	0	22.5
7	0	45
8	0	45
9	0	45
10	45	0
11	45	0
12	45	0
13	45	22.5
14	45	22.5
15	45	22.5
16	45	45
17	45	45
18	45	45

References

- [1] C. Druzgalski, A. Ashby, G. Guss, W. King, T.T. Roehling, M.J. Matthews, Process optimization of complex geometries using feed forward control for laser powder bed fusion additive manufacturing, *Additive Manufacturing* 34 (2020) 101169.
- [2] A. Prihar, S. Gupta, H.S. Esmaeeli, R. Moini, Tough double-bouligand architected concrete enabled by robotic additive manufacturing, *Nature Communications* 15(1) (2024) 7498.
- [3] Q. Liu, C. Duan, F. Richter, W. Shen, D. Wu, Interfacial behavior between thermoplastics and thermosets fabricated by material extrusion-based multi-process additive manufacturing, *Additive Manufacturing* 96 (2024) 104568.
- [4] C. Cao, X. Xia, X. Shen, X. Wang, Z. Yang, Q. Liu, C. Ding, D. Zhu, C. Kuang, X. Liu, Ultra-high precision nano additive manufacturing of metal oxide semiconductors via multi-photon lithography, *Nature Communications* 15(1) (2024) 9216.
- [5] C.V. Funch, G. Proust, Laser-based additive manufacturing of refractory metals and their alloys: A review, *Additive Manufacturing* 94 (2024) 104464.
- [6] B. Blakey-Milner, P. Gradl, G. Snedden, M. Brooks, J. Pitot, E. Lopez, M. Leary, F. Berto, A. Du Plessis, Metal additive manufacturing in aerospace: A review, *Materials & Design* 209 (2021) 110008.
- [7] S. Chandra, C. Wang, S.B. Tor, U. Ramamurty, X. Tan, Powder-size driven facile microstructure control in powder-fusion metal additive manufacturing processes, *Nature Communications* 15(1) (2024) 3094.
- [8] Y. Liao, F. Rubbi, B. Mao, B. Li, F. Delzendehrooy, M.M. Haque, A novel solid-state metal additive manufacturing process—Laser-induced Supersonic Impact Printing (LISIP): Exploration of process capability, *Additive Manufacturing* 93 (2024) 104356.
- [9] A. Du Plessis, I. Yadroitsava, I. Yadroitsev, Effects of defects on mechanical properties in metal additive manufacturing: A review focusing on X-ray tomography insights, *Materials & Design* 187 (2020) 108385.

- [10] N. Korshunova, I. Papaioannou, S. Kollmannsberger, D. Straub, E. Rank, Uncertainty quantification of microstructure variability and mechanical behavior of additively manufactured lattice structures, *Computer Methods in Applied Mechanics and Engineering* 385 (2021) 114049.
- [11] S. Mahadevan, P. Nath, Z. Hu, Uncertainty quantification for additive manufacturing process improvement: recent advances, *ASCE-ASME Journal of Risk and Uncertainty in Engineering Systems, Part B: Mechanical Engineering* 8(1) (2022) 010801.
- [12] J. Liu, B. Jalalahmadi, Y. Guo, M.P. Sealy, N. Bolander, A review of computational modeling in powder-based additive manufacturing for metallic part qualification, *Rapid Prototyping Journal* 24(8) (2018) 1245-1264.
- [13] M. Seifi, A. Salem, J. Beuth, O. Harrysson, J.J. Lewandowski, Overview of materials qualification needs for metal additive manufacturing, *Jom* 68 (2016) 747-764.
- [14] J. Torres, A.P. Gordon, Mechanics of the small punch test: a review and qualification of additive manufacturing materials, *Journal of Materials Science* 56 (2021) 10707-10744.
- [15] S. Nakarmi, J.A. Leiding, K.-S. Lee, N.P. Daphalapurkar, Predicting non-linear stress-strain response of mesostructured cellular materials using supervised autoencoder, *Computer Methods in Applied Mechanics and Engineering* 432 (2024) 117372.
- [16] C. Yang, Y. Kim, S. Ryu, G.X. Gu, Prediction of composite microstructure stress-strain curves using convolutional neural networks, *Materials & Design* 189 (2020) 108509.
- [17] C. Duan, D. Wu, Predicting stress-strain relationships of additively manufactured materials under compression and tension using transfer learning and Wasserstein distance-based dataset pruning, *Materials & Design* (2025) 114209.
- [18] Q. Liu, D. Wu, Machine learning and feature representation approaches to predict stress-strain curves of additively manufactured metamaterials with varying structure and process parameters, *Materials & Design* 241 (2024) 112932.
- [19] C. Wang, X.P. Tan, S.B. Tor, C. Lim, Machine learning in additive manufacturing: State-of-the-art and perspectives, *Additive Manufacturing* 36 (2020) 101538.
- [20] D. Fullington, E. Yangué, M.M. Bappy, C. Liu, W. Tian, Leveraging small-scale datasets for additive manufacturing process modeling and part certification: Current practice and remaining gaps, *Journal of Manufacturing Systems* (2024).
- [21] Y. Tang, M.R. Dehaghani, G.G. Wang, Review of transfer learning in modeling additive manufacturing processes, *Additive Manufacturing* 61 (2023) 103357.
- [22] F.G. Fischer, M.G. Zimmermann, N. Praetzsch, C. Knaak, Monitoring of the powder bed quality in metal additive manufacturing using deep transfer learning, *Materials & Design* 222 (2022) 111029.
- [23] Y. Tang, M. Rahmani Dehaghani, P. Sajadi, G.G. Wang, Selecting subsets of source data for transfer learning with applications in metal additive manufacturing, *Journal of Intelligent Manufacturing* (2024) 1-22.
- [24] Y. Yan, F. Wang, C. Tian, W. Xue, L. Lin, W. Cao, L. Qiao, Transfer learning and source domain restructuring-based BiLSTM approach for building energy consumption prediction, *International Journal of Green Energy* (2024) 1-15.
- [25] J. Ngiam, D. Peng, V. Vasudevan, S. Kornblith, Q.V. Le, R. Pang, Domain adaptive transfer learning with specialist models, *arXiv preprint arXiv:1811.07056* (2018).
- [26] L. Ge, J. Gao, H. Ngo, K. Li, A. Zhang, On handling negative transfer and imbalanced distributions in multiple source transfer learning, *Statistical Analysis and Data Mining: The ASA Data Science Journal* 7(4) (2014) 254-271.
- [27] M. Müller, Dynamic time warping, *Information retrieval for music and motion* (2007) 69-84.

- [28] D.J. Berndt, J. Clifford, Using dynamic time warping to find patterns in time series, Proceedings of the 3rd international conference on knowledge discovery and data mining, 1994, pp. 359-370.
- [29] S. Hochreiter, Long Short-term Memory, Neural Computation MIT-Press (1997).
- [30] W. Choi, J. Cho, S. Lee, Y. Jung, Fast constrained dynamic time warping for similarity measure of time series data, IEEE access 8 (2020) 222841-222858.
- [31] A. International, Standard test method for tensile properties of plastics, ASTM international2014.
- [32] Q. Luo, N. Huang, T. Fu, J. Wang, D.L. Bartles, T.W. Simpson, A.M. Beese, New insight into the multivariate relationships among process, structure, and properties in laser powder bed fusion AlSi10Mg, Additive Manufacturing 77 (2023) 103804.
- [33] A.I.C.E.-o.M. Testing, Standard test methods for tension testing of metallic materials, ASTM international2021.
- [34] Q. Luo, L. Yin, T.W. Simpson, A.M. Beese, Effect of processing parameters on pore structures, grain features, and mechanical properties in Ti-6Al-4V by laser powder bed fusion, Additive Manufacturing 56 (2022) 102915.
- [35] V.-A. Silvestru, I. Ariza, J. Vienne, L. Michel, A.M.A. Sanchez, U. Angst, R. Rust, F. Gramazio, M. Kohler, A. Taras, Performance under tensile loading of point-by-point wire and arc additively manufactured steel bars for structural components, Materials & Design 205 (2021) 109740.